Nodeless d-wave pairing in a two-layer Hubbard model

Nejat Bulut and Douglas J. Scalapino
Institute for Theoretical Physics, University of California, Santa Barbara, California 93106

Richard T. Scalettar
Physics Department, University of California, Davis, California 95616

(Received 7 October 1991)

Pairing correlations in a two-layer Hubbard model are studied using (1) an Eliashberg-like approximation for the exchange of spin fluctuations and (2) quantum Monte Carlo simulations. A possible pair structure in which the gap has one sign on the bonding and the opposite sign on the antibonding Fermi surface is found. Some implications of this for the transport properties of the cuprate superconductors are discussed.

I. INTRODUCTION

While various calculations have shown that many of the normal-state properties of the cuprate superconductors can be understood within the framework of a two-dimensional Hubbard model, the nature of the superconducting state and the mechanism for pairing remain a puzzle.[1] Diagrammatic calculations using an interaction obtained from the exchange of an antiferromagnetic spin fluctuation lead to a low temperature $d_{x^2-y^2}$-wave pairing instability for a doped two-dimensional (2D) Hubbard model.[2–5] Recent Monte Carlo calculations of the particle-particle vertex[6] show, for the lattice size and temperatures reached in the simulation, that there is an attractive pairing interaction in the $d_{x^2-y^2}$ channel. However, only short-range $d_{x^2-y^2}$ pair-field correlations have been seen in these simulations.[7] One might argue that the tendency toward pairing is increased when a next-nearest-neighbor one-electron hopping is included.[8] Indeed, such a term is expected from the oxygen-oxygen overlap and has been shown to enhance the $d_{x^2-y^2}$ pair-field susceptibility.[9] Nevertheless, it remains difficult to reconcile the temperature dependence of the Knight shifts[10–12] and the penetration depth[13] in $YBa_2Cu_3O_{7-\delta}$ with a gap that has nodes.

Here we study a two-layer Hubbard model in which a one-electron hopping $t_\perp$ couples the layers and gives rise to bonding and antibonding Fermi (p_x,p_y) surfaces. Within an Eliashberg-like calculation based on the exchange of spin fluctuations, we find parameter regimes in which the dominant pairing instability has a gap that is positive on one Fermi surface and negative on the other. Such a nodeless d_z-wave gap gives rise to unusual transport properties which are discussed in the conclusion.

In Sec. II we show the bonding and antibonding Fermi surfaces for several one-electron parameterizations of the band structure of the two-layer model. Then we discuss the magnetic spin susceptibility and the pair-field susceptibilities, comparing Monte Carlo results with random-phase-approximation (RPA)–Eliashberg calculations for the half-filled band where the fermion determinant is positive. In Sec. III, based upon the results of Sec. II, we study the Bethe-Salpeter equations for the pair field. Here we find parameter regimes in which the pair field with the most unstable eigenvalue has d_z symmetry. Implications of this for the transport properties of this two-layer model and some comments on the possible relationship of these ideas to the cuprate oxide superconductors are contained in Sec. IV.

II. THE TWO-LAYER MODEL AND SOME COMPARISONS WITH MONTE CARLO RESULTS

For a two-layer, two-dimensional Hubbard model, with an intralayer nearest-neighbor hopping t and an interlayer nearest-neighbor hopping $2t_\perp$, the single-particle band energy is

$$\varepsilon_{\mathbf{p}}=-2t(\cos p_x+\cos p_y)-2t_\perp\cos p_z \ . \tag{1}$$

Here p_z can take on the values 0 and π. Figure 1(a) shows the bonding ($p_z=0$) and antibonding ($p_z=\pi$) Fermi surfaces for $\langle n\rangle=1.0$ and $t_\perp=0.4t$. Throughout this paper we will measure energies in units of t. If an intralayer next-nearest-neighbor hopping t' is introduced,

$$\varepsilon_{\mathbf{p}}=-2t(\cos p_x+\cos p_y)-4t'\cos p_x\cos p_y-2t_\perp\cos p_z \ . \tag{2}$$

In this case a variety of Fermi surfaces can be produced. Figure 1(b) shows the Fermi surfaces which are found for $t_\perp=0.4t$, $t'=-0.2t$, and a site filling $\langle n\rangle=0.85$.

In the presence of an interlayer hopping $t_\perp$, the peak in the magnetic spin susceptibility $\chi(\mathbf{q},i\omega_m=0)$ shifts from having $q_z=0$ to $q_z=\pi$. Here,

$$\chi(\mathbf{q},i\omega_m=0)=\int_0^\beta d\tau\langle m_{\mathbf{q}}^-(\tau)m_{\mathbf{q}}^+(0)\rangle \ , \tag{3}$$

with

$$m_{\mathbf{q}}^+=\frac{1}{\sqrt{N}}\sum_{\mathbf{p}} c_{\mathbf{p}+\mathbf{q}\uparrow}^\dagger c_{\mathbf{p}\downarrow} \tag{4}$$

and N equal to the total number of lattice sites. Results for $\chi(\mathbf{q},0)$ for $\mathbf{q}=(\pi,\pi,\pi)$ and $(\pi,\pi,0)$ obtained from a Monte Carlo simulation of a $2\times(4\times4)$ Hubbard lattice are shown in Fig. 2. Here $U=4t$, $t_\perp=0.4t$, $t'=0$, and $\mu=0$, corresponding to a half-filled band having particle-hole symmetry so that there is no *determinental* sign problem. The Fermi surface corresponding to this case is shown in Fig. 1(a). As the temperature is lowered, we see that the dominant spin-spin correlations have $q_z=\pi$.

The solid and dashed curves in Fig. 2 show results obtained using an RPA form,

$$\chi(\mathbf{q},i\omega_m)=\frac{\chi_0(\mathbf{q},i\omega_m)}{1-\bar{U}\chi_0(\mathbf{q},i\omega_m)}\ , \tag{5}$$

with

$$\chi_0(\mathbf{q},i\omega_m)=\frac{1}{N}\sum_{\mathbf{p}}\frac{f(\varepsilon_{\mathbf{p}+\mathbf{q}})-f(\varepsilon_{\mathbf{p}})}{i\omega_m-(\varepsilon_{\mathbf{p}+\mathbf{q}}-\varepsilon_{\mathbf{p}})}\ . \tag{6}$$

Here $\bar{U}=2.35t$ is an effective Coulomb interaction adjusted so as to fit the RPA form to the Monte Carlo results. Physically, the introduction of $\bar{U}$ takes into account the correlated particle-particle t-matrix scattering and self-energy effects.

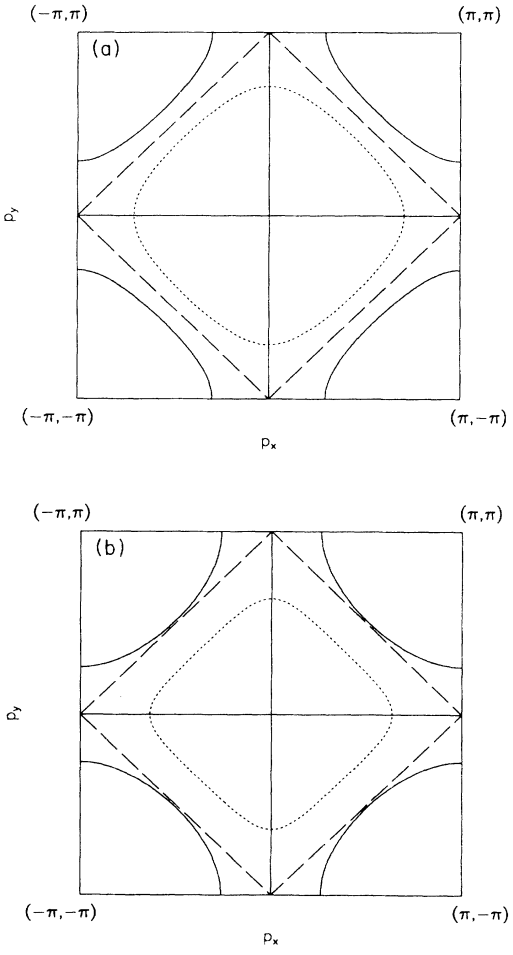

FIG. 1. Fermi surfaces for a two-layer model corresponding to $p_z=0$ (solid curve) and $p_z=\pi$ (dotted curve). Here (a) $t_\perp=0.4t$, $t'=0$, $\mu=0$ ($\langle n\rangle=1.0$) and (b) $t_\perp=0.4t$, $t'=-0.2t$, $\mu=-0.7t$ corresponding to $\langle n\rangle=0.85$. The long dashed curve shows the Fermi surface for $t_\perp=t'=0$ and $\langle n\rangle=1.0$.

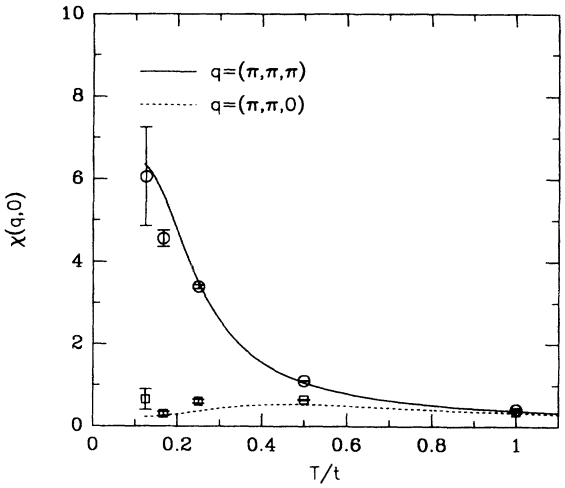

FIG. 2. Monte Carlo results for $\chi(\pi,\pi,\pi)$ (circles) and $\chi(\pi,\pi,0)$ (squares) vs T on a $2\times(4\times4)$ lattice for $U=4t$, $t_\perp=0.4t$, $t'=0$, and $\mu=0$. The lines are RPA fits with $\bar{U}=2.35t$.

To examine the pairing interaction, we have calculated the pair-field correlation functions

$$P_\alpha=\frac{1}{N}\int_0^\beta d\tau\langle\Delta_\alpha(\tau)\Delta_\alpha^\dagger(0)\rangle\ , \tag{7}$$

for

$$\Delta^\dagger_{x^2-y^2}=\sum_{\mathbf{p}}(\cos p_x-\cos p_y)c^\dagger_{\mathbf{p}\uparrow}c^\dagger_{-\mathbf{p}\downarrow} \tag{8}$$

and

$$\Delta_z^\dagger=\sum_{\mathbf{p}}\cos p_z c^\dagger_{\mathbf{p}\uparrow}c^\dagger_{-\mathbf{p}\downarrow}\ . \tag{9}$$

Monte Carlo results for P_α are shown in Figs. 3(a) and 3(b). The squares show the pair-field susceptibilities in the absence of interaction vertices,[14]

$$\bar{P}_\alpha=\frac{1}{N}\sum_{\mathbf{p}}g_\alpha^2(\mathbf{p})\int_0^\beta d\tau\, G_{\mathbf{p}\uparrow}(\tau)G_{-\mathbf{p}\downarrow}(\tau)\ , \tag{10}$$

and the circles show P_α, Eq. (7), which includes the full effect of the interactions. From Figs. 3(a) and 3(b) one sees that the interaction is attractive in both the $d_{x^2-y^2}$, $g_\alpha=(\cos p_x-\cos p_y)$, and d_z, $g_\alpha=\cos p_z$, particle-particle channels.

Within the RPA, the effective singlet particle-particle interaction mediated by the exchange of a spin fluctuation,[15] illustrated in Fig. 4, is

$$V(p'|p)=U+\frac{\bar{U}^2\chi_0(p'+p)}{1-\bar{U}\chi_0(p'+p)}+\frac{\bar{U}^3\chi_0^2(p'-p)}{1-\bar{U}^2\chi_0^2(p'-p)}\ , \tag{11}$$

where p represents $(\mathbf{p},i\omega_n)$. Here $\chi_0(\mathbf{q},i\omega_m)$ is given by Eq. (6) and $\bar{U}$ is the effective Coulomb interaction. Note in this expression that the first term U must be the bare

Coulomb interaction since $V(p'|p)$ is to be used in a particle-particle ladder graph. We have used this interaction, Eq. (11), within a Migdal-Eliashberg-like approximation,[16] illustrated in Fig. 5, to calculate P_α and $\bar{P}_\alpha$. The results are shown as the solid and dashed curves for P_α and $\bar{P}_\alpha$, respectively, in Figs. 3(a) and 3(b). In this approximation, vertex corrections are neglected and the parameters in the basic spin-fluctuation exchange interaction, Eq. (11), are set by adjusting $\bar{U}$ so that the RPA form for $\chi(\mathbf{q},i\omega_m)$ fits the Monte Carlo results for $\chi(\mathbf{q},i\omega_m)$. In addition, the single-particle Green's function $G(\mathbf{p},i\omega_n)$ is dressed with the spin-fluctuation self-energy shown in Fig. 6.

This approach is similar in spirit to the early work on electron-phonon mediated superconductivity in which the vertex corrections were neglected and the phonon propagator was fit to the neutron scattering data. In the present case, however, one does not have the usual Migdal result which supported the neglect of the electron-phonon vertex corrections. While there is a small parameter involving the spin-fluctuation energy compared to the Fermi energy, the strong momentum dependence arising from the near nesting of the Fermi surface raises questions. We have, however, looked at the effect of the lowest-order vertex corrections and find numerically that they introduce relatively small changes[17] in P_α for the lattice sizes and temperatures considered here, consistent with the comparisons shown in Figs. 3(a) and 3(b). This encourages us to extend this type of approximation to study the Bethe-Salpeter equation for the pair field discussed in Sec. III. Basically, we will use an effective $\bar{U}$ to parametrize the interaction equation (11) and neglect vertex corrections. The full momentum and Matsubara frequency dependence will be kept and the single-particle Green's-function self-energy will be calculated self-consistently.

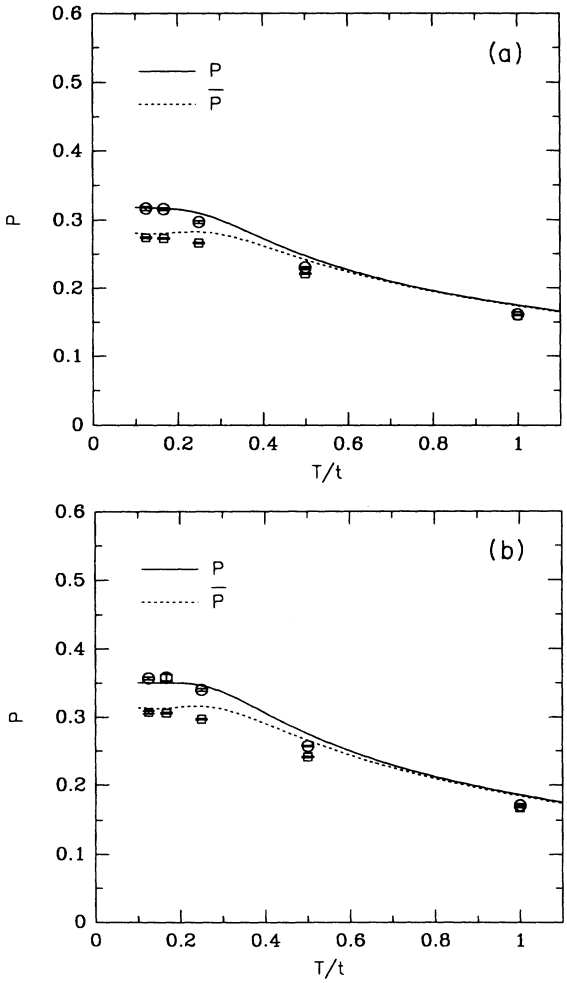

FIG. 3. Pair-field susceptibilities (a) P_z and (b) $P_{x^2-y^2}$ vs T for $t_\perp=0.4t$, $t'=0$, and $\langle n\rangle=1.0$. The points are quantum Monte Carlo (QMC) data with $U=4t$, and the lines are RPA results with $\bar{U}=2.35t$. Here the circles and the solid line represent P_α with the Coulomb vertex corrections, and the squares and the dotted line represent $\bar{P}_\alpha$ without the vertex corrections.

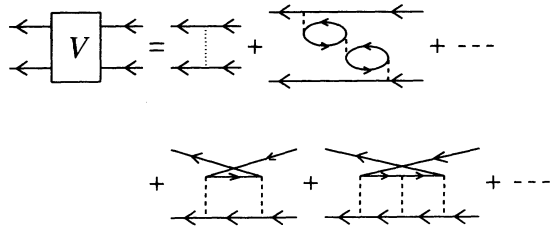

FIG. 4. RPA spin-fluctuation contribution to the even-parity singlet interaction. Here, the dotted line represents the bare Coulomb repulsion U, and the dashed line represents the reduced Coulomb repulsion $\bar{U}$.

III. THE BETHE-SALPETER EQUATION

As we have seen, there is an attractive interaction in both the $d_{x^2-y^2}$ and d_z pairing channels. In order to explore in more detail the structure of the pairing correlations induced by the spin-fluctuation exchange potential $V(p'|p)$, Eq. (11), we have solved the Bethe-Salpeter equation shown in Fig. 7:

$$\lambda\phi(\mathbf{p},i\omega_n)=-\frac{T}{N}\sum_{\mathbf{p}',n'}V(\mathbf{p},i\omega_n|\mathbf{p}',i\omega_{n'})G(\mathbf{p}',i\omega_{n'})\times G(-\mathbf{p}',-i\omega_{n'})\phi(\mathbf{p}',i\omega_{n'})\ . \quad (12)$$

Here, just as before, vertex corrections are neglected, and the single-particle Green's function $G(\mathbf{p},i\omega_n)$ is self-consistently dressed with the spin-fluctuation self-energy, (see Fig. 6). We will examine the singlet solution with $\phi(\mathbf{p},i\omega_n)=\phi(-\mathbf{p},-i\omega_n)$.

The frequency dependence of $\phi(\mathbf{p},i\omega_n)$ reflects the structure of the underlying spin-fluctuation interaction. However, the momentum dependence is a function of the structure of $\chi_0(\mathbf{q})$. If the two Fermi surfaces are such that $\chi_0(\mathbf{q})$ peaks for $q_z=0$, the eigenfunction with the largest eigenvalue has $d_{x^2-y^2}$ wave symmetry. In leading order $\phi(\mathbf{p})\approx\cos p_x-\cos p_y$ on both sheets. If, however,

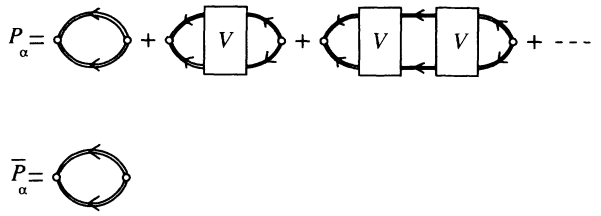

FIG. 5. Migdal-Eliashberg approximations for P_α and $\bar{P}_\alpha$.

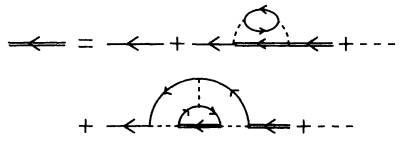

FIG. 6. Spin-fluctuation contribution to the self-energy of the single-particle Green's function.

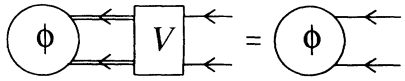

FIG. 7. Bethe-Salpeter equation for the gap function $\phi(\mathbf{p}, i\omega_n)$.

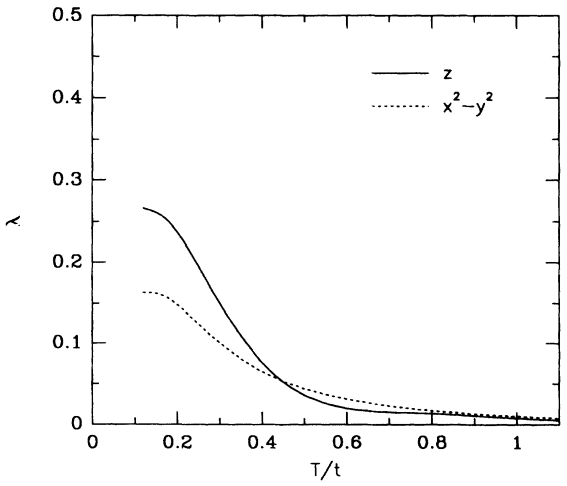

FIG. 8. Temperature dependence of the eigenvalues λ_z (solid curve) and $\lambda_{x^2-y^2}$ (dotted curve) of the Bethe-Salpeter equation for a $2\times(4\times4)$ lattice with $t_\perp=0.4t$, $t'=0$, $U=4t$, $\bar{U}=2.35t$, and $\mu=0$.

the Fermi surfaces are such that $\chi_0(\mathbf{q})$ peaks for $q_z=\pi$, then the eigenfunction with the largest eigenvalue will have one sign on the bonding and the opposite sign on the antibonding Fermi surface. Neglecting the additional variations with p_x and p_y, this corresponds to a gap with $\cos p_z$ symmetry and in terms of the site operators

$$\Delta_z^\dagger = \sum_{\mathbf{p}} \cos(p_z) c_{\mathbf{p}\uparrow}^\dagger c_{-\mathbf{p}\downarrow}^\dagger = \tfrac{1}{2} \sum_l (c_{l\uparrow}^\dagger c_{\bar{l}\downarrow}^\dagger - c_{l\downarrow}^\dagger c_{\bar{l}\uparrow}^\dagger) . \quad (13)$$

Here $c_{l\uparrow}^\dagger$ creates an electron with spin up on the upper lattice at site $l=(l_x,l_y)$ and $c_{\bar{l}\downarrow}^\dagger$ creates an electron with spin down directly below it on the lower lattice.

Our solution of the Bethe-Salpeter equation was carried out on a finite lattice with a cutoff on the allowed Matsubara frequencies. As the temperature is lowered, the eigenvalues of the Bethe-Salpeter equation increase. The transition temperature is determined by the tempera-

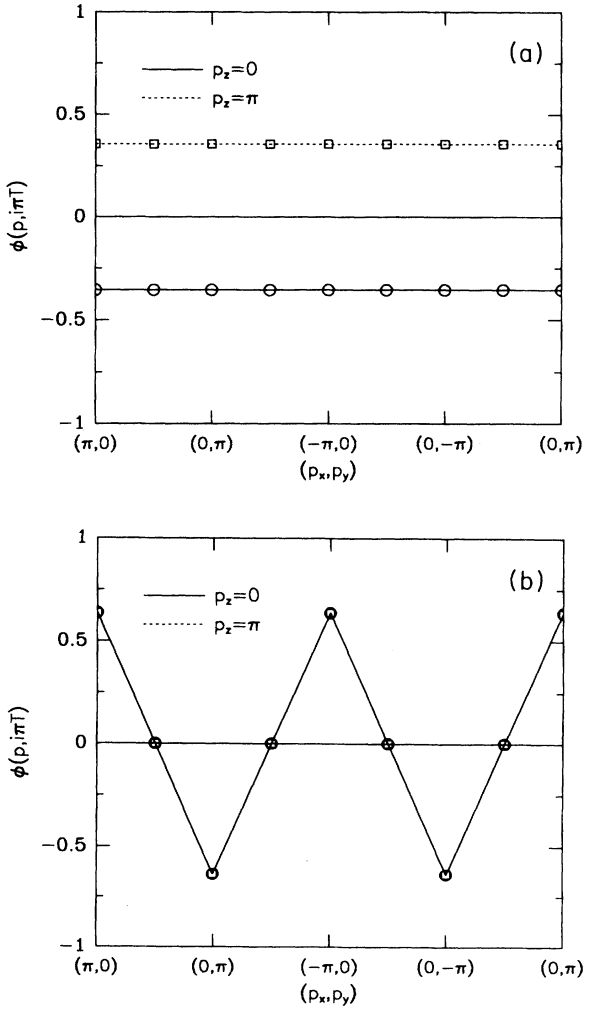

FIG. 9. Momentum dependence of the gap function for (a) d_z- and (b) $d_{x^2-y^2}$-wave symmetries on a $2\times(4\times4)$ lattice with $t_\perp=0.4t$, $t'=0$, $u=4t$, $\bar{U}=2.35t$, $\mu=0$, and $T=0.10t$. Note that for the $d_{x^2-y^2}$ symmetry shown in (b) the solid and dashed lines lay on top of each other within the resolution of this figure.

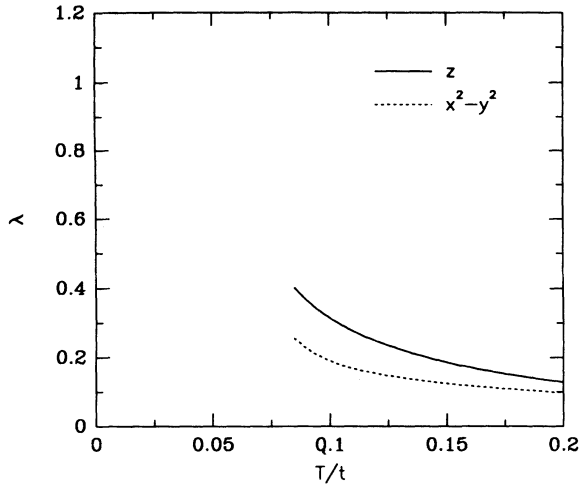

FIG. 10. Same as in Fig. 8, but on a $2\times(8\times8)$ lattice for $t_\perp=0.4t$, $t'=-0.2t$, $U=4t$, $\bar{U}=2.35t$, and $\langle n\rangle=0.85$.

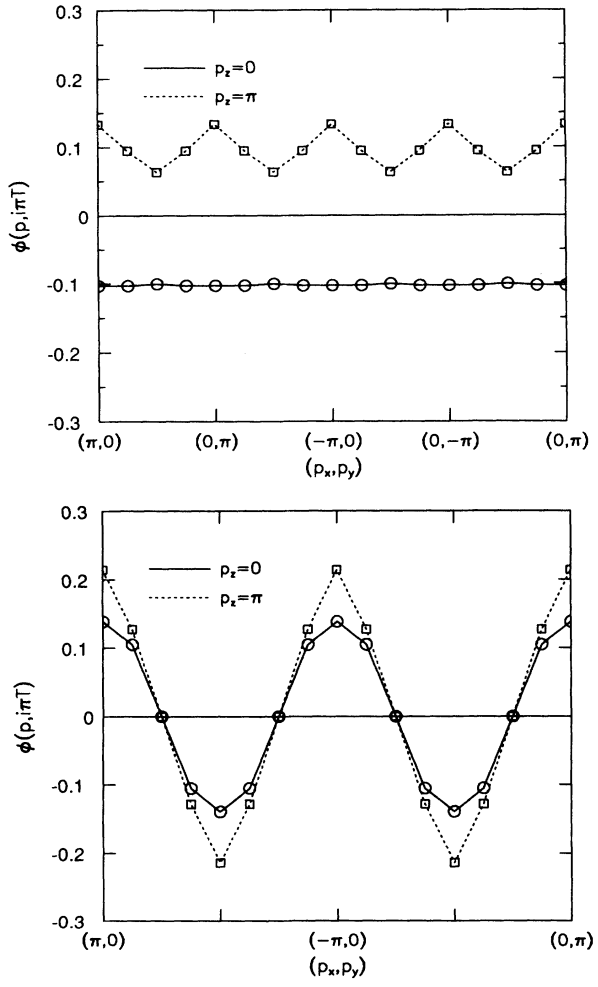

FIG. 11. Same as in Fig. 9, but on a $2\times(8\times8)$ lattice for $t_\perp=0.4t$, $t'=-0.2t$, $U=4t$, $\bar{U}=2.35t$, $\langle n\rangle=0.85$, and $T=0.10t$.

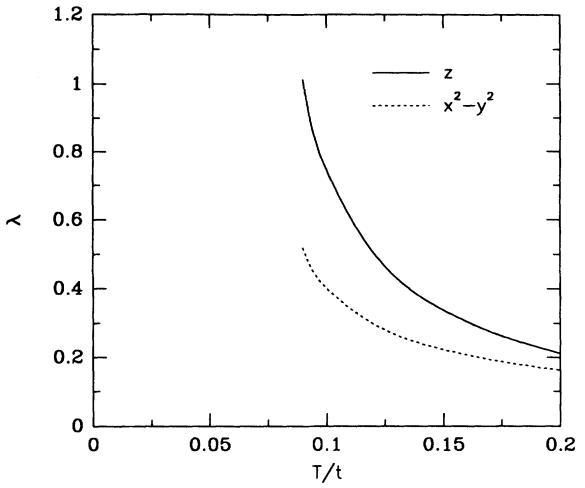

FIG. 12. Same as in Fig. 10, but here $\lambda_z(T)$ and $\lambda_{x^2-y^2}(T)$ have been calculated without taking into account the self-energy due to spin fluctuations.

ture at which the largest eigenvalue reaches unity.[18]

For the parameters considered in Sec. II, $t_\perp=0.4t$, $t'=0$, and $\mu=0$, the temperature dependences of the two largest eigenvalues are shown in Fig. 8. This calculation has been done on a 4×4 lattice with $\bar{U}=2.35t$ as determined from Sec. II and a frequency cutoff of $10t$. At low temperatures, the largest eigenvalue is λ_z. The momentum dependence of its eigenfunction $\phi(\mathbf{p},i\omega_n)$ for $\omega_n=\omega_1=\pi T$ is shown in Fig. 9(a). It has one sign on the bonding and the opposite sign on the antibonding Fermi surface, corresponding to $\cos(p_z)$. The momentum dependence of the eigenfunction associated with the second largest eigenvalue, $\lambda_{x^2-y^2}$, is shown in Fib. 9(b). Its behavior is essentially $\cos(p_x)-\cos(p_y)$.

We have also solved the Bethe-Salpeter equation away from half-filling. It is possible to find parameter regimes where the d_z-wave pair-field correlations grow faster than those having $d_{x^2-y^2}$-wave symmetry, as the temperature is lowered. In Fig. 10 we show $\lambda_z(T)$ and $\lambda_{x^2-y^2}(T)$ for one such set of parameters: $\langle n\rangle=0.85$, $U=4t$, $\bar{U}=2.35t$, $t_\perp=0.4t$, and $t'=-0.2t$. This calculation has been done on a $2\times(8\times8)$ lattice using a frequency cutoff of $5t$. The corresponding eigenfunctions $\phi(\mathbf{p},i\pi T)$ versus $\mathbf{p}$ are plotted in Figs. 11(a) and 11(b). They are similar to Figs. 9(a) and 9(b).

In the model that we are using, the antiferromagnetic correlations can affect the pair-field correlations in two ways: the spin-fluctuation exchange potential of Eq. (11) is roughly proportional to χ; hence strong AF correlations enhance the eigenvalues λ. However, they can also suppress λ through their effect on the single-particle self-energy.[2,19] Figure 12 shows $\lambda_z(T)$ and $\lambda_{x^2-y^2}(T)$ calculated by neglecting the spin-fluctuation self-energy. Comparison of Fig. 12 with Fig. 10 gives a clear indication of the strong suppression of λ_z and $\lambda_{x^2-y^2}$ by the self-energy.

IV. CONCLUSIONS

For a two-layer Hubbard model, we have seen that the interlayer coupling can lead to a magnetic susceptibility $\chi(\pi,\pi,\pi)$ that exceeds $\chi(\pi,\pi,0)$, reflecting the interlayer antiferromagnetic correlations. Furthermore, within a Migdal-Eliashberg-like approximation, using an interaction mediated by the exchange of spin fluctuations, we have found that the pairing correlations can favor a gap that has one sign on the bonding Fermi surface and an opposite sign on the antibonding Fermi surface. This allows a spin-fluctuation exchange interaction that is repulsive in momentum space to produce a singlet pairing state without nodes on the Fermi surface.

As is well known, $YB_2Cu_3O_{7-\delta}$ contains a stack of weakly coupled bilayers. However, these bilayers are separated by a layer of Y atoms, and the Cu atoms in the different planes of a bilayer have no intervening oxygen atom. Thus, the magnetic coupling between layers occurs via direct exchange rather than a superexchange interaction. Nevertheless, the neutron scattering is found to be modulated on a scale set by the bilayer separation,[20] reflecting the interlayer antiferromagnetic spin-spin correlations. In addition, band-structure calculations[21] give a Fermi surface which consists of bonding and antibonding cylinders (along with quasi-one-dimensional sheets arising from the chains). Thus, it is possible that the gap could have one sign on the bonding and the opposite sign on the antibonding cylinder. Similarly, one could imagine alternating signs for the gap on the three degenerate Fermi-surface cylinders of $Tl_2Ba_2Ca_2Cu_3O_{10}$.

The single-layer materials such as $La_{2-x}Sr_xCuO_4$ would apparently require a gap with nodes. However, within the framework we have been considering in which the one-electron interactions separate the Fermi surface into different sheets, it may be that the octahedral tilting creates a Fermi surface consisting of separate pieces on which the gap can have opposite signs. This picture of a "nodeless d wave" is similar to that proposed by Schrieffer, Wen, and Zhang.[22] However, they envisioned that the modification of the Fermi surface arose dynamically from self-energy effects associated with the spin-fluctuation interaction, while we are suggesting that the one-electron band potential is responsible for creating the appropriate pieces of the Fermi surface.

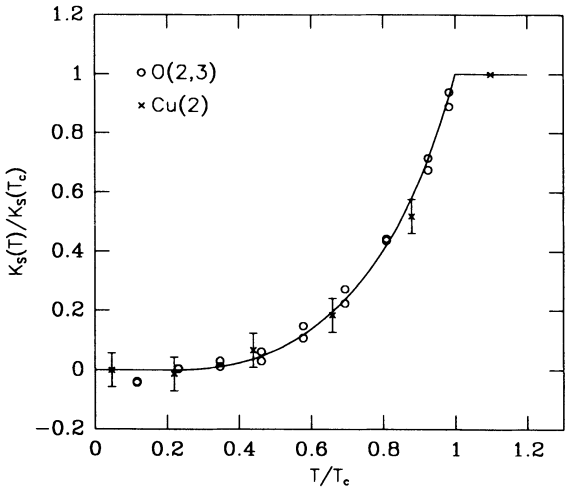

FIG. 13. Temperature dependence of the Knight shift for d_z-wave gap symmetry. Here $t_\perp = t' = 0$, $\langle n \rangle = 0.86$, $U = 2t$, $2\Delta(0) = 4kT_c$, and $T_c = 0.10t$. The crosses are the experimental Knight shift data on Cu(2) by Barrett *et al.* (Ref. 10), and the circles are the O(2,3) data by Takigawa *et al.* (Refs. 11 and 12).

As noted in the Introduction, this work was in part motivated by the question of whether a d-wave superconducting state, which arose from the exchange of spin fluctuations, could provide a consistent explanation for the observed transport properties. Here we conclude by examing some transport properties for a simple phenomenological model in which the gap $\Delta_{\mathbf{p}}$ has opposite signs on the bonding and antibonding Fermi surfaces:

$$\Delta_{(p_x,p_y,0)} = -\Delta_{(p_x,p_y,\pi)} = \Delta(T) , \tag{14}$$

and $\Delta(T)$ has the usual BCS temperature dependence. In the following we will assume that $t_\perp/t$ is sufficiently small and that the bonding and antibonding Fermi surfaces are essentially degenerate.

As shown in Sec. III and previously discussed, an RPA form for $\chi(\mathbf{q},i\omega_m)$ with an effective $\bar{U}$ can provide a parametrization of the susceptibility. Extending this to the superconducting state by replacing $\chi_0(\mathbf{q},i\omega_m)$, Eq. (4), by the BCS form

$$\begin{aligned}\chi_0^{\mathrm{BCS}}(\mathbf{q},i\omega_m) = \frac{1}{N}\sum_{\mathbf{p}} \Bigg[& \frac{1}{2}\left[1+\frac{\varepsilon_{\mathbf{p}+\mathbf{q}}\varepsilon_{\mathbf{p}}+\Delta_{\mathbf{p}+\mathbf{q}}\Delta_{\mathbf{p}}}{E_{\mathbf{p}+\mathbf{q}}E_{\mathbf{p}}}\right]\frac{f(E_{\mathbf{p}+\mathbf{q}})-f(E_{\mathbf{p}})}{i\omega_m-(E_{\mathbf{p}+\mathbf{q}}-E_{\mathbf{p}})} \\ & +\frac{1}{4}\left[1-\frac{\varepsilon_{\mathbf{p}+\mathbf{q}}}{E_{\mathbf{p}+\mathbf{q}}}+\frac{\varepsilon_{\mathbf{p}}}{E_{\mathbf{p}}}-\frac{\varepsilon_{\mathbf{p}+\mathbf{q}}\varepsilon_{\mathbf{p}}+\Delta_{\mathbf{p}+\mathbf{q}}\Delta_{\mathbf{p}}}{E_{\mathbf{p}+\mathbf{q}}E_{\mathbf{p}}}\right]\frac{1-f(E_{\mathbf{p}+\mathbf{q}}-f(E_{\mathbf{p}})}{i\omega_m+(E_{\mathbf{p}+\mathbf{q}}+E_{\mathbf{p}})} \\ & +\frac{1}{4}\left[1+\frac{\varepsilon_{\mathbf{p}+\mathbf{q}}}{E_{\mathbf{p}+\mathbf{q}}}-\frac{\varepsilon_{\mathbf{p}}}{E_{\mathbf{p}}}-\frac{\varepsilon_{\mathbf{p}+\mathbf{q}}\varepsilon_{\mathbf{p}}+\Delta_{\mathbf{p}+\mathbf{q}}\Delta_{\mathbf{p}}}{E_{\mathbf{p}+\mathbf{q}}E_{\mathbf{p}}}\right]\frac{f(E_{\mathbf{p}+\mathbf{q}})+f(E_{\mathbf{p}})-1}{i\omega_m-(E_{\mathbf{p}+\mathbf{q}}+E_{\mathbf{p}})}\Bigg]\end{aligned} \tag{15}$$

represents the simplest approximation that takes into account both the antiferromagnetic and superconducting correlations.[23] Then the Knight shift $K_S(T)$ is just proportional to the $\mathbf{q}\to 0$, $\omega_m = 0$ limit of $\chi(\mathbf{q},i\omega_m)$,

$$\chi(0,0) = \frac{\chi_0^{\mathrm{BCS}}(0,0)}{1-\bar{U}\chi_0^{\mathrm{BCS}}(0,0)} , \tag{16}$$

with

$$\chi_0^{\rm BCS}(0,0)=\frac{1}{N}\sum_{(p_x,p_y)} f(E_{\rm p}) , \tag{17}$$

the usual Yosida function. Since $E_{\rm p}=\sqrt{\varepsilon_{\rm p}^2+\Delta_{\rm p}^2}$, the low-temperature dependence follows the standard BCS behavior. Results for $\bar{U}=2t$ and $2\Delta(0)/kT_c=4$ are compared with the experimental data[10–12] in Fig. 13. The Stoner enhancement factor $[1-\bar{U}\chi_0^{\rm BCS}(0,0)]^{-1}$ is of order 1.7 at T_c and decreases to 1 as T drops below T_c.[23] This produces a more rapid falloff of $K_s(T)/K_S(T_c)$ than the simple Yosida function which would require a $2\Delta(0)/kT_c$ ratio of order 5 to fit the data without the Stoner factor. We find that the low-temperature behavior of the penetration depth has the same nodeless behavior as K_S, reflecting the nonzero magnitude of the gap.

The fact that the gap has one sign on the bonding and the opposite on the antibonding Fermi surface leads to a suppression[24] of the Hebel-Slichter peak in the nuclear relaxation rate T_1^{-1} of both the Cu and O. Using the analytic continuation of $\chi(\mathbf{q},i\omega_m)$, T_1^{-1} for a nominal spin-$\frac{1}{2}$ system is given by

$$T_1^{-1}=\frac{T}{N}\sum_{\mathbf{q}} |A(\mathbf{q})|^2 \frac{{\rm Im}\chi(\mathbf{q},\omega)}{\omega}\bigg|_{\omega\simeq 0} . \tag{18}$$

Here $|A(\mathbf{q})|^2$ is the appropriate hyperfine form factor for the Cu(2) or O(2,3) nuclei. Using the same RPA parametrization of $\chi(\mathbf{q},\omega)$ and the Mila-Rice[25] form factor $|A(\mathbf{q})|^2$ that was previously used to fit the normal-state $T>T_c$ data,[26] we have calculated T_1^{-1} for $T<T_c$ with $\chi_0^{\rm BCS}$ and the gap from Eq. (14).[27] Results for T_1^{-1} for Cu and O are compared with experiment in Figs. 14(a) and 14(b). We note, however, that while the dip in the $(T_1^{-1})_{ab}/(T_1^{-1})_c$ anisotropy ratio of the Cu(2) relaxation rate below T_c is reproduced by the form of the gap given in Eq. (14), the subsequent rise of this ratio observed experimentally[28] and predicted[23] for a $d_{x^2-y^2}$ gap is not present.

Within this model for $\Delta_{\rm p}$, we find that the $\mathbf{q}\sim 0$ microwave conductivity $\sigma_1(\nu,T)$ exhibits the usual Hebel-Slichter peak.[29,30] This may be further enhanced if the quasiparticle lifetime increases below T_c, as discussed by Nuss *et al.*[30]

Finally, we conclude by noting that for this form of the gap, the neutron scattering intensity for momentum transfer near $\mathbf{Q}=(\pi,\pi,\pi)$ will exhibit a sharp peak at

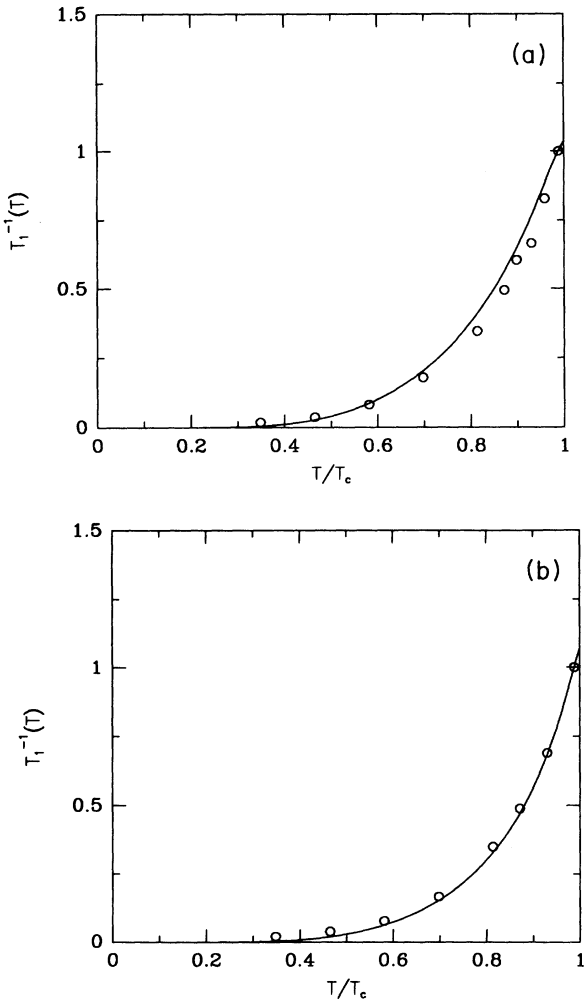

FIG. 14. Temperature dependence of the (a) O(2,3) and (b) Cu(2) nuclear relaxation rates for a d_z-wave gap symmetry. The points are the experimental data (Refs. 32 and 12) taken in an orienting magnetic field of $8T$ along the c axis, which reduces T_c to 86 K. Since the experimental value of T_1^{-1} at $T_c=86$ K is not available, we have renormalized T_1^{-1} by its value at $T=85$ K. The parameters used to fit the data are $t_\perp=t'=0$, $\langle n\rangle=0.86$, $U=2t$, $\Gamma(T)=0.6T_c(T/T_c)^3$, $2\Delta_0=5kT_c$ and $T_c=0.10t$.

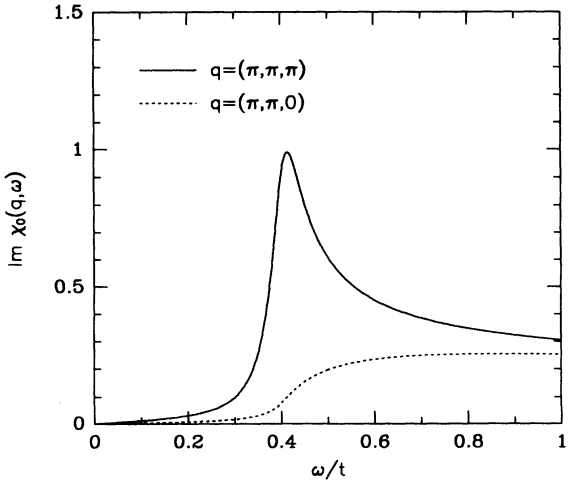

FIG. 15. Spin-fluctuation spectral function ${\rm Im}\chi(\mathbf{q},\omega)$ vs ω for the $U=0$ system at $\mathbf{q}=(\pi,\pi,\pi)$ (solid curve) and $\mathbf{q}=(\pi,\pi,0)$ (dotted curve). Here the parameters are $t_\perp=t'=0$, $\langle n\rangle=1.0$, $T=0.02t$, and $\Delta_0=0.20t$.

$\omega \sim 2\Delta(T)$ in contrast to the gradual onset for an s-wave gap. This is because $\Delta_{\mathbf{p}+\mathbf{Q}} = -\Delta_{\mathbf{p}}$ so that the coherence factor at threshold is unity rather than zero, while the density of states has its usual square-root singularity.[31] In Fig. 15, we illustrate this by plotting $\mathrm{Im}\chi_0(\mathbf{q},\omega)$, the solid curve, versus ω for $\mathbf{q}=(\pi,\pi,\pi)$ at half-filling. If the momentum transfer is changed to $(\pi,\pi,0)$ (the dotted curve), the usual gradual s-wave-like onset is seen. Thus, this difference in the threshold behavior for these two momentum transfers would provide a signature for the type of the gap structure described in this paper.

ACKNOWLEDGMENTS

We would like to acknowledge useful discussions with F. Müller, W. Pickett, and L. Sham regarding the Fermi surfaces and band structure of the cuprate superconductors. We would also like to acknowledge useful discussions with R. Klemm on layered superconductors.[33] This work was partially supported by the National Science Foundation under Grant Nos. DMR90-02492 and PHY89-04035, and by the Electric Power Research Institute. The numerical calculations reported in this paper were performed at the San Diego Supercomputer Center.

[1] *High Temperature Superconductivity,* edited by K. S. Bedell, D. Coffey, D. Meltzer, D. Pines, and J. R. Schrieffer (Addison-Wesley, Reading, MA, 1990); M^{2}S-HTSC III Proceedings [Physica (Utrecht) (to be published)].

[2] N. E. Bickers, D. J. Scalapino, and R. T. Scalettar, Int. J. Mod. Phys. B **1**, 687 (1987); N. E. Bickers, D. J. Scalapino, and S. R. White, Phys. Rev. Lett. **62**, 961 (1989).

[3] H. Shimahara and S. Takada, J. Phys. Soc. Jpn. **57**, 1044 (1988).

[4] P. Monthoux, A. Balatsky, and D. Pines, Phys. Rev. Lett. **67**, 3448 (1991).

[5] K. Ueda, T. Moriya, and Y. Takahashi (unpublished).

[6] S. R. White *et al.* (unpublished).

[7] M. Imada and Y. Hatsugai, J. Phys. Soc. Jpn. **58**, 3752 (1989); A. Moreo and D. J. Scalapino, Phys. Rev. B **43**, 8211 (1991); N. Furukawa and M. Imada, M^{2}S-HTSC III Proceedings [Physica (Utrecht) (to be published)].

[8] J. E. Hirsch and D. J. Scalapino, Phys. Rev. Lett. **56**, 2732 (1986).

[9] R. R. dos Santos, Phys. Rev. B **39**, 7259 (1989).

[10] S. E. Barrett *et al.*, Phys. Rev. B **41**, 6283 (1990).

[11] M. Takigawa, P. C. Hammell, R. H. Heffner, and Z. Fisk, Phys. Rev. B **39**, 7371 (1989).

[12] M. Takigawa, P. C. Hammel, R. H. Heffner, Z. Fisk, K. C. Ott, and J. D. Thompson, Physica (Amsterdam) **162-164C**, 853 (1989).

[13] D. R. Harshmann *et al.*, Phys. Rev. B **39**, 851 (1989); R. L. Greene, L. Krusin-Elbaum, and A. P. Malozemoff, Phys. Rev. Lett. **62**, 2886 (1989).

[14] S. R. White *et al.*, Phys. Rev. B **39**, 839 (1989).

[15] N. F. Berk and J. R. Schrieffer, Phys. Rev. Lett. **17**, 433 (1966).

[16] A. B. Migdal, Zh. Eksp. Teor. Fiz. **34**, 1438 (1958) [Sov. Phys. JETP **7**, 996 (1958)]; G. M. Eliashberg, Zh. Eksp. Teor. Fiz. **38**, 966 (1960) [Sov. Phys. JETP, **11**, 696 (1960)].

[17] This is in agreement with K. Yonemitsu, J. Phys. Soc. Jpn., **58**, 4576 (1989).

[18] In order to go to low temperatures, larger lattices and more Matsubara frequencies are required. Further work is in progress to do this as well as to compare P_α and $\bar{P}_\alpha$ with Monte Carlo results on larger lattices to explore the reliability of the approximation scheme described in this paper.

[19] A. J. Millis, S. Sachdev, and C. M. Varma, Phys. Rev. B **37**, 4975 (1988).

[20] J. M. Tranquada, *Proceedings of the University of Miami Workshop on Electronic Structure and Mechanisms for High Temperature Superconductivity,* edited by J. Ashkenazi and G. Vezzoli (Plenum, New York, 1991).

[21] W. E. Pickett, Rev. Mod. Phys. **61**, 433 (1989).

[22] J. R. Schrieffer, X.-G. Wen, and S. C. Zhang, Phys. Rev. B, **39**, 11 663 (1989). These authors propose that the pairing mechanism arises from an attractive interaction coming from second-order processes involving the crossed exchange of two spin fluctuations.

[23] D. J. Scalapino, *High Temperature Superconductivity* (Ref. 1); N. Bulut and D. J. Scalapino, Phys. Rev. B (to be published).

[24] This behavior which is associated with the effect of the gap symmetry, Eq. (8), in the coherence factors has been discussed for a $d_{x^2-y^2}$ gap in Ref. 23.

[25] F. Mila and T. M. Rice, Physica (Amsterdam) **157C**, 561 (1989).

[26] N. Bulut, D. Hone, D. J. Scalapino, and N. E. Bickers, Phys. Rev. B **41**, 1797 (1990); Phys. Rev. Lett. **64**, 2723 (1990).

[27] A quasiparticle damping rate $\Gamma = 0.6T_c(T/T_c)^3$ was also included.

[28] J. A. Martindale, S. E. Barrett, C. A. Klug, K. E. O'Hara, S. M. DeSoto, C. P. Slichter, T. A. Friedmann, and D. M. Ginsberg (unpublished); M. Takigawa, J. L. Smith, and W. L. Hults (unpublished).

[29] K. Holczer *et al.* (unpublished).

[30] M. C. Nuss *et al.*, Phys. Rev. Lett. **66**, 3305 (1991).

[31] N. Bulut and D. J. Scalapino (unpublished).

[32] P. C. Hammell, M. Takigawa, R. H. Heffner, Z. Fisk, and K. C. Ott, Phys. Rev. Lett. **63**, 1992 (1989).

[33] R. A. Klemm and S. H. Liu, Phys. Rev. B **44**, 7526 (1991).